Available online at www.sciencedirect.com
ScienceDirect
Optics Communications 281 (2008) 1156–1161
OPTICS COMMUNICATIONS
www.elsevier.com/locate/optcom

Stability properties of current-profiled quantum dot lasers

John Houlihan [a,b,*], Carmel Kelleher [b]

[a] Department of Computing, Maths and Physics, Waterford Institute of Technology, Waterford, Ireland
[b] Tyndall National Institute, Lee Maltings, Cork, Ireland

Received 17 August 2007; accepted 17 October 2007

Abstract

The stability properties of injection-current profiled quantum dot lasers are analyzed for broad area devices of different length. In general, devices demonstrate stable output at low to moderate injection levels before the onset of filamentary dynamics at higher injection levels. By comparing devices of different lengths, the onset of filamentary dynamics is shown to coincide in each case with the onset of excited state lasing and so the loss in stability may be linked to the increased low frequency noise and phase-amplitude coupling that occurs in this regime.

1. Introduction

Quantum dot (QD) based photonic materials are currently receiving a large amount of attention due to the interesting blend of atomic and solid state properties that they possess [1]. By fabricating semiconductor lasers (SLs) from such materials, researchers have demonstrated devices that exhibit temperature insensitive, low threshold currents [1], high modulation bandwidths [2,3] and a low sensitivity to optical feedback [4]. In addition, semiconductor optical amplifiers (SOAs) fabricated from such materials are expected to provide new opportunities for ultrafast data processing [5], while monolithic mode locked lasers made from QD materials have demonstrated enhanced jitter performance [6]. QD SLs have also demonstrated improved beam quality over their quantum well (QW) counterparts, exhibiting reduced filamentation [7,8] and superior M^2 values up to 45 mW in output power [9].

The general improvement in QD SLs when compared to QW devices is due to their unique carrier dynamics which results in a reduced phase-amplitude coupling (α-parameter) [10,11] and increased relaxation oscillation damping [4,12], both factors contributing to a non-linear system less sensitive to internal/external perturbations [13]. The aim of this paper is to investigate how QD materials can improve the stability of spatially extended laser devices towards providing coherent emission in the multi-Watt range.

The study of the evolution of complexity and pattern formation in spatially extended systems has many examples in nonlinear optics [14] and in particular SLs [15–19]. Conventional QW and QD spatially extended lasers usually display unstable filamentary dynamics once the injection increases beyond twice the laser threshold [20]. In Ref. [21], a simple technique was presented to suppress this instability based on spatially varying the pump by patterning the contact electrode of the device. A related technique was later developed, which involved the inclusion of an additional current spreading layer to allow the injection profile to diffuse from a flat profile at injection to a smoothened, bell shaped profile in the active region [22]. In pulsed, non-thermal operation, the device displayed a stable dual-lobed far-field and diffraction limited beam waist to ten times threshold. Each lobe in the far-field corresponded to a spatially separate transverse traveling wave in the near-field, stabilized by the smooth, carrier-induced, refractive index anti-guide [23]. The possibility of generating off-axis emission with such injection profiling was first

* Corresponding author. Address: Department of Computing, Maths and Physics, Waterford Institute of Technology, Waterford, Ireland. Tel.: +353 21 490 4852; fax: +353 21 427 6949.
E-mail address: jhoulihan@wit.ie (J. Houlihan).

0030-4018/$ - see front matter © 2007 Elsevier B.V. All rights reserved.
doi:10.1016/j.optcom.2007.10.048

identified by Petermann [24]. Operation of the device in continuous-wave mode resulted in the evolution of a thermally-induced positive waveguide, which negated the carrier-induced anti-guide for increasing currents and thereby collapsed the stable non-linear mode of the cavity with unstable filamentary dynamics resulting [25]. In this paper, the effect of such injection profiling on the modal properties of a spatially extended QD device is examined.

2. Epitaxial structure and device

The epitaxial structure for our device was supplied by Innolume (formerly Nanosemiconductor GMBH) and contained 10 layers of MBE grown InAs QDs on a GaAs substrate. Each QD layer was formed by growing an 0.8 nm thick InAs QD layer on a 33 nm thick GaAs wetting layer and capped with a 5 nm thick layer of $In_{0.15}Ga_{0.85}As$. Surrounding the active region was a 500 nm thick $Al_{0.35}Ga_{0.65}As$ n-(p-)type Si(C) doped layer ($5\times10^{17}\,cm^{-3}$), a 1000 nm thick $Al_{0.35}Ga_{0.65}As$ n-(p-)type Si(C) doped layer ($1\times10^{18}\,cm^{-3}$) and a 15 nm thick $Al_xGa_{1-x}As$ (x graded from 0.35 to 0) layer, n-(p-)type Si(C) doped to $3\times10^{18}\,cm^{-3}$. The n-side contained an additional 300 nm thick GaAs layer doped to $3\times10^{18}\,cm^{-3}$. To achieve current spreading p-side contained a 2000 nm thick GaAs layer doped to $2\times10^{19}\,cm^{-3}$ and a 100 nm thick capping layer, doped to $1\times10^{20}\,cm^{-3}$. It should be noted that the previously used spreading layer was an MOVPE grown 10 μm thick, 4×10^{18} doped GaAs layer [22]; to achieve spreading in the MBE grown QD wafer, a thinner, more highly doped layer was used. Broad area lasers were fabricated by defining narrow injection stripes and devices of two different lengths, 1.5 mm and 3 mm were tested.

A typical spontaneous emission profile at the emitting facet is shown in Fig. 1 and indicates the amount of carrier spreading present in the device. The carriers have spread from 5 μm at the injection stripe to 120 μm in the active region. It should be noted that the amount of spreading experienced in the present quantum dot wafer is more than the comparable QW device previously studied where a 5 μm injection stripe resulted in an 80 μm FWHM spontaneous emission profile [22].

To analyze the modal properties of the QD lasers, far-field, near-field and beam waist measurements were performed on devices of two different lengths. The devices were operated in pulsed regime (1 kHz repetition rate, 100 ns pulse width) to avoid self heating effects and isolate the carrier field interplay. The stability of the optical field was inferred by examining the beam waist measurements where loss of spatial coherence causes dramatic broadening and loss of symmetry.

3. Short device: 1.5 mm

Far-field intensity distributions for the 1.5 mm long device are shown in Fig. 2. At lower currents the far-field consists of two lobes symmetrically placed about the optical axis, similar to those previously observed in current-profiled QW lasers [23]. In the QW case, the inter-lobe divergence was determined by the strength of the refractive index anti-guide and was constant as the current increased due to the combination of a carrier density clamped at threshold and a constant phase-amplitude coupling (α-factor). However, in the present QD case, the inter-lobe divergence first increases as the current increases before decreasing at higher currents. These changes in the inter-lobe divergence reflect the above threshold changes in the phase-amplitude coupling due to changes in the non-resonant carrier densities, as previously described by Dagens et al. [26] and explained in [27]. At 2 A injection current, the on-axis region of the far field has begun to "fill-in" and, by 2.5 A no discernible structure remains in the far-field distribution.

The corresponding beam waist distributions are displayed in Fig. 3. At lower currents, the profiles consist of a narrow central lobe, with symmetrically placed minor side lobes. Again, these profiles are very similar to those previously reported for the QW case and indicate coherent

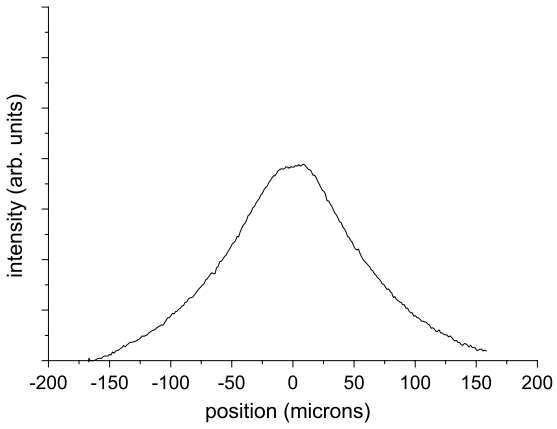

Fig. 1. Near-field spontaneous emission profile from 5 μm injection stripe width device (120 mA pump current, FWHM 120 μm).

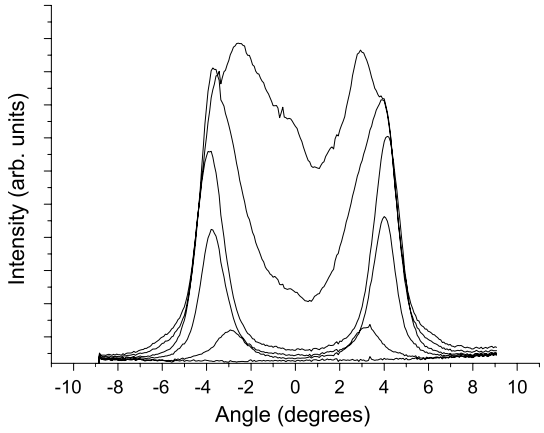

Fig. 2. Far-field intensity distributions from short device for increasing currents (500 mA, 1 A, 1.5 A, 2 A, 2.5 A).

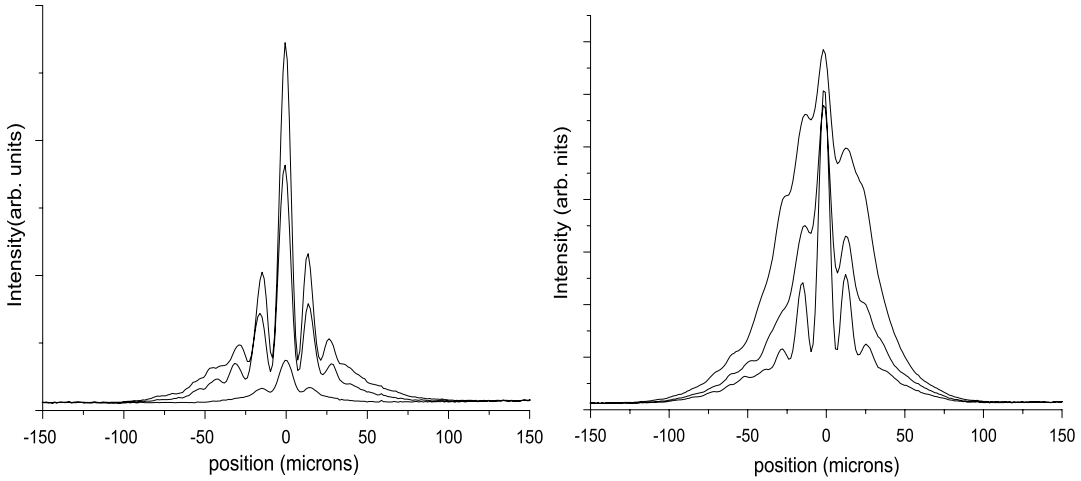

Fig. 3. Beam waist intensity distributions from short device for increasing currents (left – 400 mA, 800 mA, 1 A, right – 1.5 A, 2 A, 2.5 A).

output of the device. However, as with the far-field distributions, the shape exhibits qualitative changes by 2 A, having broadened and lost symmetry about the optic axis, the narrow side lobes being barely discernible. The broadening continues to 2.5 A and is indicative of a loss in the coherence of the device due to unstable, filamentary output.

The near-fields for this device are shown in Fig. 4 for various currents. Below threshold, the near-field displays a smooth, bell shaped profile which reflects the smoothened carrier profile in the active region due to the current spreading layer as mentioned previously. At lower currents above threshold, the near-field also follows the injection

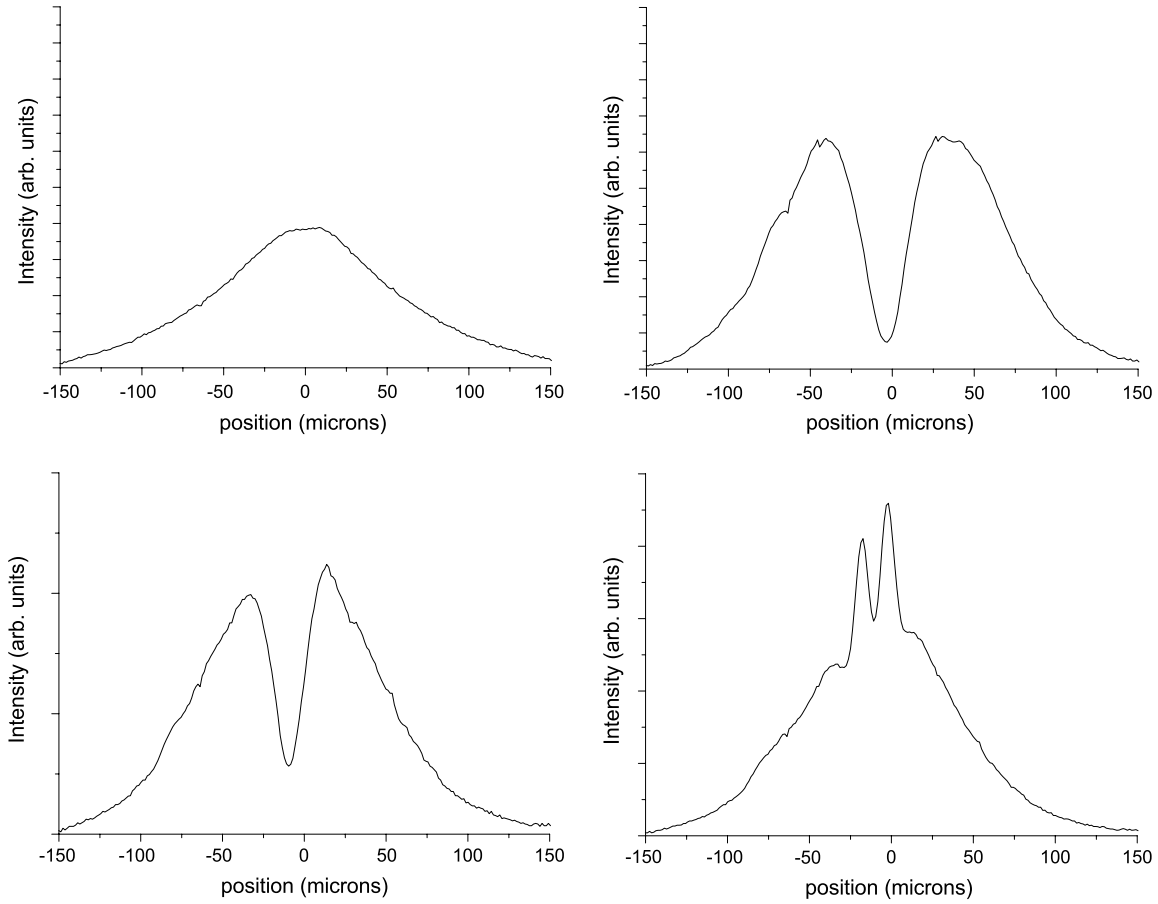

Fig. 4. Near-field intensity distributions from short device for various currents (top left 120 mA, top right 1.2 A, bottom left 2 A, bottom right 2.5 A).

profile apart from a central defect where very little light is present. By varying the distance between the facet and imaging lens it is possible to track the evolution of the beam from its waist to near field and onto the far-field. By performing such an observation at lower currents above threshold, it was noted that the near-field lobes propagate to the far-field lobes without crossing, as would be expected from the presence of a carrier-induced anti-guide. Such a near-field profile is similar to that observed in the QW case where each lobe in the far-field was associated with a spatially distinct region of the near-field. However, the defect region was not visible in the QW case. At increased injection, the near-field begins to lose its symmetry about the optical axis and the defect region begins to fill in. At 2.5 A, where both beam waist and far-field exhibit evidence for loss in spatial coherence and unstable output, the near-field exhibits the formation of filament-like structures in the central region. The injection current level at which stable, coherent output collapses to unstable emission was estimated to be 1.7 A by observing the evolution and broadening of the near, far and beam waist fields.

To further investigate the cause(s) for the onset of unstable behavior in the present QD structure, the optical spectrum of the device was recorded over its range of operation and is displayed in Fig. 5. For the lowest current level the device is below threshold, and the resulting spontaneous emission profile is maximized at the ground state transition near 1290 nm and broadened by two effects, inhomogeneous broadening due to dot size irregularity and the presence of a first excited state transition near 1180 nm. As the current increases, lasing at the ground state is apparent and increases steadily until 1.5 A. At this current, lasing is also beginning to occur for the excited state, and becomes progressively stronger as the current increases to 2.5 A. This onset of excited state lasing has been reported previously in QD structures [28] and has been explained as a consequence of the reduced effective mass of holes in the dot structure. As a result, the hole energy level spacing is reduced to a degree where, at room temperature, holes in the dot can be said to occupy a single shared hole level [29]. The onset of two state lasing is usually accompanied by an increase in the phase-amplitude coupling due to increased complexity of the gain spectrum [26] and an increase in the noise properties of the device due to the increased degree of freedom as well as α-factor changes [30]. The destabilization of the current-profiled quantum dot devices may be a further consequence of these increases.

4. Long device: 3.0 mm

To examine the relationship between the onset of excited state lasing and the collapse of stable, coherent output of the device, a longer device was tested. Increasing the length of the device allows it to reach threshold at a reduced current density and thus delay the onset of excited state lasing to higher currents. However, it should be noted that increasing the length of an optical cavity, without changing the width of the cavity results in a decrease in the Fresnel number (F) of the cavity and thus a reduction in the number of available modes of the 2-d cavity ($F = \frac{a^2}{L\lambda}$, where a is the width of the cavity, L is the length and λ is the wavelength of the laser). To partially compensate for this reduction, our longer device was chosen to have a larger injection region which corresponded to a spontaneous emission FWHM of 150 μm in comparison to the 120 μm FWHM of the 1.5 mm device.

The far-field intensity distribution resulting from the longer device is shown in Fig. 6 at various currents up to 6 A. As with the shorter device, the main feature is the dual-lobed pattern, with a central region which begins to fill for high currents (>3.7 A). Also the inter-lobe divergence is not constant above threshold (as was previously the case with QW structures), but initially increases before decreasing for higher currents, again reflecting the changing phase-amplitude coupling above threshold.

The corresponding beam waist intensity distributions are shown in Fig. 7. At a current of 1 A, the distribution

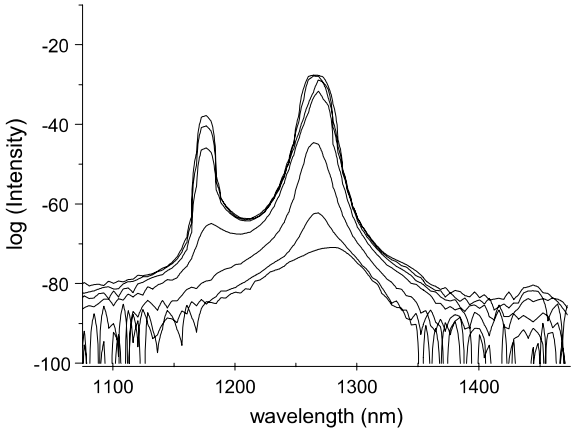

Fig. 5. Optical spectra from short device for increasing currents (0.1 A, 0.2 A, 0.4 A, 1 A, 1.5 A, 2 A, 2.5 A).

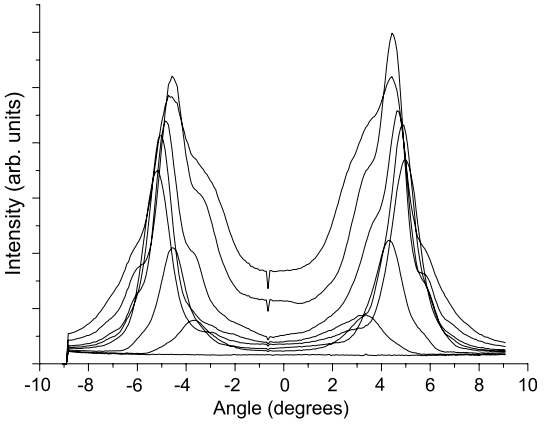

Fig. 6. Far-field intensity distributions from long device for various currents (1 A, 2 A, 3 A, 3.7 A, 4 A, 5 A, 6 A).

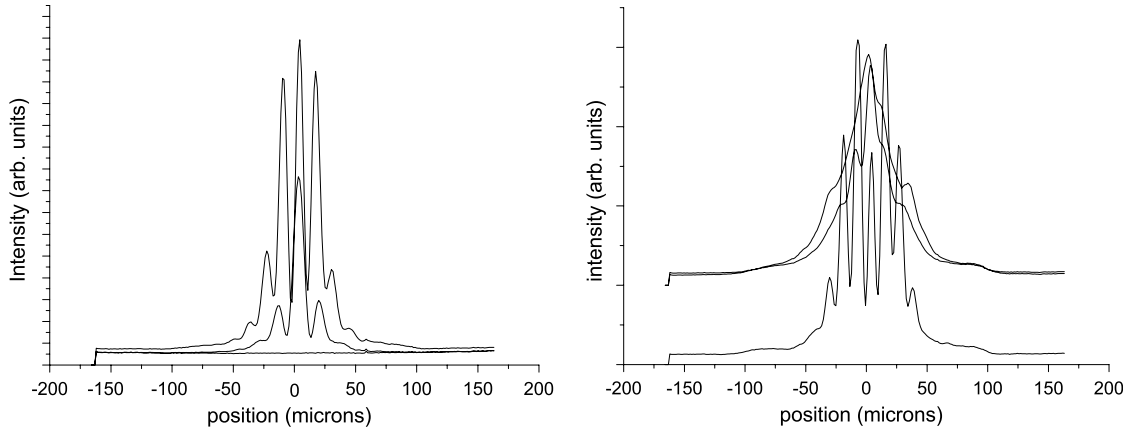

Fig. 7. Beam waist intensity distributions from long device for various currents (left – 1 A, 2 A, right – 3 A, 4 A, 5 A (some vertically offset for clarity)).

is very similar to the short laser case, consisting of a main central lobe and minor symmetric side lobes. As the current increased, these side lobes also increased, however the symmetry of the shape remained and the visibility of the lobes indicate the absence of unstable filamentary dynamics in this current range. Above currents of 3.7 A, the shape become much more complicated, with the side lobes losing their symmetry and collapsing to a broad featureless distribution indicating the loss of stability and coherence and the onset of filamentary dynamics.

The near-field intensity distributions for this device are shown in Fig. 8. For the lowest current, the broad 150 μm FWHM spontaneous emission profile is apparent. For lower currents above threshold, near-fields similar to the shorter device occur. These exhibit lasing on either side of the device with reduction in the center, albeit in a less symmetric fashion. At the highest currents, the central region fills, and filament-like features appear. To summarize the results for the longer device, the injection current level at which stable, coherent output collapses to unstable emission was estimated to be 3.7 A, primarily determined by the loss of visibility of the fringes in the beam waist intensity distribution.

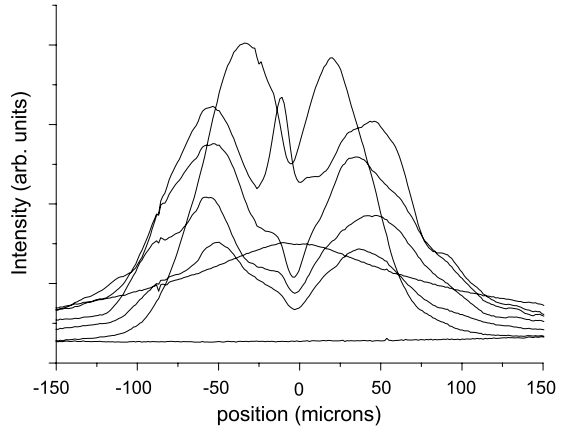

Fig. 8. Near-field intensity distributions from long devices at various currents (0.2 A, 0.5 A, 2 A, 3 A, 4.5 A, 5 A).

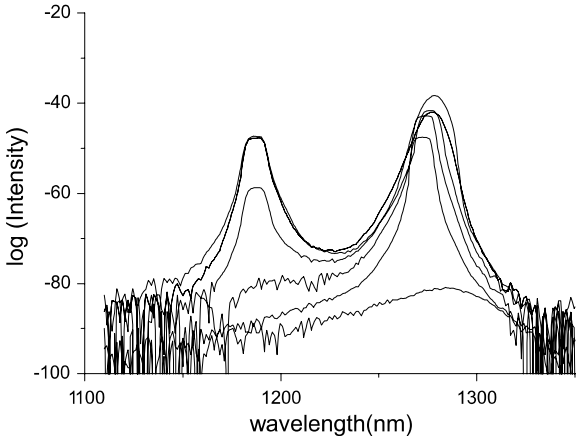

Fig. 9. Optical spectra of long device for various currents (0.2 A, 1 A, 2 A, 3 A, 4 A, 5 A).

To further compare with the shorter device, the spectrum of the longer device is shown in Fig. 9. The below threshold, spontaneous emission spectrum is similar to that observed in the shorter device and the evolution as current is increased is similar (though occurs over a wider range of currents due to the increased length of the device). Most notably, the current at which the device output become unstable and filamentary is linked to the onset of excited state lasing in a similar fashion to the shorter device, even though this current is much higher in the longer case (3.7 A) than in the shorter case (1.7 A). Thus, in both the long and short devices de-stabilisation of the optical field with increasing current can be associated with the onset of excited state lasing. The ensuing filamentary dynamics may be due to the increases in low frequency noise and phase-amplitude coupling that occur in this regime.

5. Conclusion

The stability properties of broad area, injection profiled, quantum dot semiconductor lasers are analyzed for devices of different length. Generally, the onset of spatio-temporal

instability coincides with the onset of excited state lasing possibly due to the increased level of noise and increased phase-amplitude coupling which occurs in this regime. As these effects are unique to quantum dot structures, this information is of importance to designers of high brightness lasers considering utilizing quantum dot materials for their noted benefits.

Acknowledgement

The authors would like to acknowledge useful discussions with Guillaume Huyet and Brian Corbett, James O'Callaghan for technical assistance and financial support from the Tyndall National Access Program (NAP).

References

[1] D. Bimberg, M. Grundmann, N.N. Ledentsov, Quantum Dot Hetero-structures, Wiley, New York, 1999.
[2] Z. Mi, P. Bhattacharya, S. Fathpour, Appl. Phys. Lett. 86 (2005) 153109.
[3] M. Kuntz, G. Fiol, M. Laemmlin, C. Schubert, A.R. Kovsh, A. Jacob, A. Umbach, D. Bimberg, IEE Electron. Lett. 41 (2005) 244.
[4] D. O'Brien, S.P. Hegarty, G. Huyet, J.G. McInerney, T. Kettler, M. Laemmlin, D. Bimberg, V.M. Ustinov, A.E. Zhukov, S.S. Mikhrin, A.R. Kovsh, IEE Electron. Lett. 39 (2003) 1819.
[5] A.V. Uskov, E.P. O'Reilly, R.J. Manning, R.P. Webb, D. Cotter, M. Laemmlin, N.N. Ledentsov, D. Bimberg, IEEE Photon. Technol. Lett. 16 (2004) 1265.
[6] M.T. Todaro, J.P. Tourrenc, S.P. Hegarty, C. Kelleher, B. Corbett, G. Huyet, J.G. McInerney, Opt. Lett. 31 (2006) 3107.
[7] P.M. Smowton, E.J. Pearce, H.C. Schneider, W.W. Chow, M. Hopkinson, Appl. Phys. Lett. 81 (17) (2002) 3251.
[8] S. Fathpour, P. Bhattacharya, S. Pradhan, S. Ghosh, IEE Electon. Lett. 39 (20) (2003) 1443.
[9] Ch. Ribbat, R.L. Sellin, I. Kaiander, F. Hopfer, N.N. Ledentsov, D. Bimberg, A.R. Kovsh, V.M. Ustinov, A.E. Zhukov, M.V. Maximov, Appl. Phys. Lett. 82 (6) (2003) 952.
[10] T.C. Newell, D.J. Bossert, A. Stintz, B. Fuchs, K.J. Malloy, L.F. Lester, IEEE Photon. Tech. Lett. 11 (12) (1999) 1527.
[11] J. Muszalski, J. Houlihan, G. Huyet, B. Corbett, IEE Electron. Lett. 40 (7) (2004) 428.
[12] M. Kuntz, N.N. Ledentsov, D. Bimberg, A.R. Kovsh, V.M. Ustinov, A.E. Zhukov, Y.M. Shernyakov, Appl. Phys. Lett. 81 (2002) 3846.
[13] D. O'Brien, S.P. Hegarty, G. Huyet, A.V. Uskov, Opt. Lett. 29 (2004) 10.
[14] F.T. Arecchi, S. Boccaletti, P.L. Ramazza, Phys. Report 318 (1999) 1, and references therein.
[15] S.P. Hegarty, G. Huyet, J.G. McInerney, K.D. Choquette, Phys. Rev. Lett. 82 (1999) 1434.
[16] I. Fischer, O. Hess, W. Elsasser, E. Gobel, Euro. Phys. Lett. 35 (1996) 579.
[17] K.F. Huang, Y.F. Chen, H.C. Lai, Y.P. Lan, Phys. Rev. Lett. 89 (2002) 224102.
[18] Y.F. Chen, K.F. Huang, H.C. Lai, Y.P. Lan, Phys. Rev. Lett. 90 (2003) 053904.
[19] E. O'Neill, J. Houlihan, J.G. McInerney, G. Huyet, Phys. Rev. Lett. 94 (2005) 143901.
[20] Y. Tanguy, J. Muszalski, J. Houlihan, G. Huyet, E.J. Pearce, P.M. Smowton, M. Hopkinson, Opt. Commun. 235 (2004) 387.
[21] C. Lindsey, P. Derry, A. Yariv, Electron. Lett. 21 (1985) 671.
[22] J.R. O'Callaghan, J. Houlihan, V. Voignier, G. Huyet, J.G. McInerney, B. Corbett, P.A. O'Brien, IEEE Photon. Tech. Lett. 14 (1) (2002) 9.
[23] V. Voignier, J. Houlihan, J.R. O'Callaghan, C. Saillot, G. Huyet, Phys. Rev. A 65 (2002) 053807.
[24] K. Petermann, Opt. Quantum Electron. 13 (1981) 323.
[25] J.R. O'Callaghan, J. Houlihan, V. Voignier, G.H. Wu, E. O'Neill, J.G. McInerney, G. Huyet, IEEE J. Quant. Electron. 40 (1) (2002) 1.
[26] B. Dagens, A. Markus, J.X. Chen, J.-G. Provost, D. Make, O. Le Gouezigou, J. Landreau, A. Fiore, B. Thedrez, Electron. Lett. 41 (6) (2005) 323.
[27] S. Melnik, G. Huyet, A.V. Uskov, Opt. Express 14 (7) (2006) 29650.
[28] A. Markus, J.X. Chen, C. Paranthoen, A. Fiore, C. Platz, O. Gauthier-Lafaye, Appl. Phys. Lett. 82 (2003) 1818.
[29] E.A. Viktorov, P. Mandel, Y. Tanguy, J. Houlihan, G. Huyet, Appl. Phys. Lett. 87 (2005) 053113.
[30] E.A. Viktorov, P. Mandel, I. O'Driscoll, O. Carroll, G. Huyet, J. Houlihan, Y. Tanguy, Opt. Lett. 31 (15) (2006) 2302.